VNU Journal of Science:
Computer Science and Communication Engineering

Journal homepage: http://www.jcsce.vnu.edu.vn/index.php/jcsce

Original Article

A Comprehensive Study of Adaptive LNA Nonlinearity Compensation Methods in Direct RF Sampling Receivers

Vu Ngoc Anh[1], Le Hai Nam[1], Tran Thi Hong Tham[2,*], Trinh Quang Kien[1]

[1]*Le Quy Don Technical University, Hanoi, Vietnam*
[2]*Moscow Institute of Physics and Technology, Moscow, Russia*

Received 21 June 2020
Revised 08 September 2020; Accepted 07 October 2020

Abstract: This paper studies the effects of nonlinear distortion of Low Noise Amplifier (LNA) in the multichannel direct-RF sampling receiver (DRF). The main focus of our work is to study and compare the effectiveness of the different adaptive compensation algorithms, including the inverse-based and subtract-based Least Mean Square (LMS) algorithm with a fixed and variable step size. The models for the compensation circuits have been analytically derived. As the major improvements, the effectiveness of the compensation circuits under the ADC quantization noise effect is evaluated. The bit-error-rates (BER) in dynamic signal-to-noise ratio (SNR) scenarios are calculated. We have proposed the use of variable step-size LMS (VLMS) to shorten the convergence time and to improve the compensation effect in general. To evaluate and compare different compensation methods, a complex Matlab model of the Ultra high frequency (UHF) DRF with 4-QPSK channels was implemented. The simulation results show that all compensation methods significantly improve the receiver performance, with the convergence time of the VLMS algorithm does not exceed 5.10^4 samples, the adjacent channel power ratios (ACPR) are reduced more than 30 dBc, and the BERs decrease by 2–3 orders of magnitude, compared with the non-compensated results. The simulation results also indicate that the subtraction method in general has better performance than the inversion method.

Keywords: Direct RF digitization, DCR, LNA distortion, digital receiver, LMS filter, multichannel receiver, software-defined radio, UHF transceiver.

1. Introduction

The Direct RF sampling receiver (DRF) is predicted to be the replacement of the superheterodyne receivers. The major distinguishing feature is that the DRF receiver digitalizes and down-converts the RF signal to the intermediate frequency (IF) without the need for an analog downsampler and mixer, hence, being a mostly all-digital receiver.

The absence of the IF analog components thoroughly eliminates conventional issues such as IQ imbalance, DC offset [1, 2]. The DRF is favorable for building up the true concept of software-defined radio [3-5], where the receiver

* Corresponding author.
E-mail address: tranhongtham@phystech.edu

https://doi.org/10.25073/2588-1086/vnucsce.257

can simultaneously operate in multichannel, multiband, multimode while maintaining a fairly simple and cost-effective design [3, 4]. Nonetheless, DRF receivers still need an LNA to amplify the received signal at the antenna. Therefore they still suffer from the LNA nonlinearity, especially for wideband and multichannel receiving. After the LNA, if the input power exceeds the 1 dB compression point as shown in Fig. 1, high power RF channels (distortion sources) would generate harmonics and intermodulation, which affect the quality of itself and low power channels [5-11]. The higher the power of distortion sources, the more serious the effect of LNA nonlinearity is, hence a correction circuit is required to compensate and restore the received channel signal quality. Estimating and compensating the distortion effects are the primary functions of the circuit.

In most of the prior arts, the solutions aim for common direct conversion receivers (DCR) and correct the distortion by canceling or inverting all the nonlinear effects, using the LS algorithm [5-8]. Based on the methods described in [5-8], two distortion correction schemes for multichannel wideband DRFs using LMS algorithm are proposed, in [12-14]. The system performance is assessed by the convergence speed of the coefficients and the spectra comparison of the distorted and the corrected signal. Sharing the similarity in the circuit topologies and methods, however, the mathematical models of the compensation circuits and their working principle have not been discussed in detail. Some important factors such as the quantization noise or the dynamic SNR scenarios were not covered in those works, which may lead to unrealistic estimation of BER performance of the proposed solutions.

In this work, we conducted a systematic study on several compensation approaches for DRF, including the adaptive distortion subtraction (ADS) and adaptive distortion inversion (ADI) schemes. Other than that, we also proposed variable step-size LMS for enhancing the convergence speed and improve the system performance, i.e., BER. All compensation approaches have been evaluated with real parameter simulation for a DRF operating in a multichannel mode. The major performance metrics, including the convergence time of LMS, extracted ACRP, and BERs, have been simulations and evaluated

The remaining of the paper is organized as follows. Section 2 presents the distortion analytical models of LNA and analyzes the effect of distortion on the multichannel DRF model with extracted parameters of a commercial LNA. Section 3 describes the LNA distortion compensation circuits using ADI and ADS with LMS and VLMS algorithms. Section 4 presents and discusses the major simulation results for a realistic receiver model and setup. The conclusions are drawn in section 5.

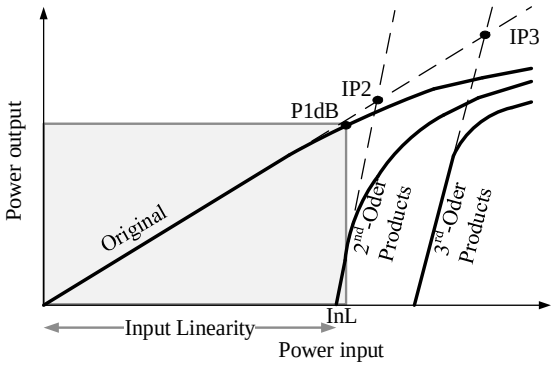

Fig. 1. LNA Input-Output power characteristics

2. Nonlinear LNA Distortions Models and Their Impacts on DRFs

2.1. LNA Nonlinear Distortion Model

The generic structure of DRF is shown in Fig. Fig. 2. The signal from the antenna first is pre-filtered by a low-pass filter (LPF) array to remove out-of-band frequencies. The band-limited signal then is amplified by the LNA before being digitalized by a high-speed ADC. Depending on the SFDR of the ADC, the LNA is required to have a suitable gain factor to ensure the receiver's sensitivity [1, 8]. The problem is, the LNAs only work linearly within

a limited input power range. When the input signal energy is out of this range, the amplifier becomes saturated and produces nonlinear distortions at the amplifier output [3-15]. There are two types of nonlinear LNA distortions that need to be taken into consideration: self-affected distortions caused by an individual RF signal to itself and distortions causes by the interference of other RF signals [3-15].

As in [10-12], the RF signal, including nonlinear components, is assumed to be a polynomial and can be expressed as (1)

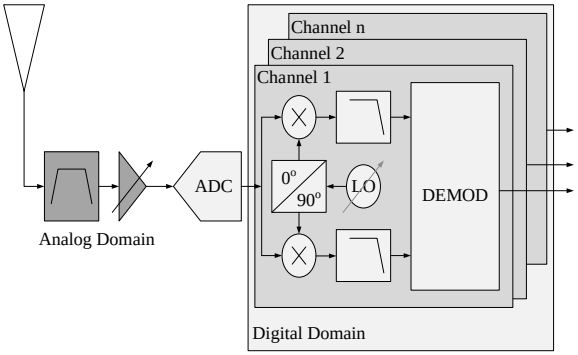

Fig. 2. The architecture of direct digitization receiver.

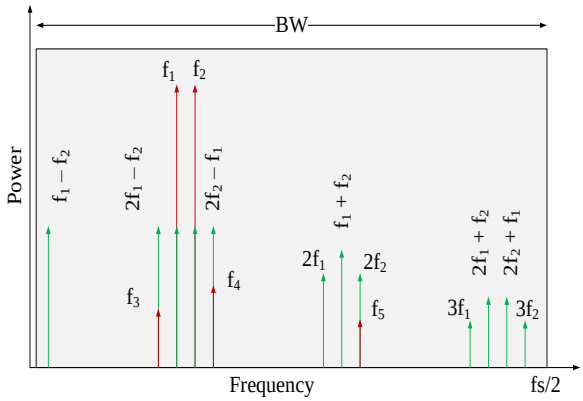

Fig. 3. The nonlinear components of LNA with two-tone input.

$$y_{RF}(t) = \sum_{i=1}^{k} a_i(t) x^i{}_{RF}(t) \qquad (1)$$

where $x_{RF}(t)$ and $y_{RF}(t)$ are LNA input and output signals respectively; $a_i(t)$ is the i[th]-order component coefficient. The input signal $x_{RF}(t)$, in turn, is represented as (2).

$$x_{RF}(t) = 2Re\left[x(t)e^{j\omega_c t}\right] = x(t)e^{j\omega_c t} + x^* e^{-j\omega_c t} \qquad (2)$$

where $x(t)$ is the baseband signal of $x_{RF}(t)$, $x(t)$ can be a single carrier frequency or multiple separate carrier frequencies. $\omega_c = 2\pi f_c$, with f_c is the center carrier frequency and (.)* represents the complex conjugate.

In DRFs, the signal of a single channel can be distorted by harmonics and intermodulation generated from far-away channels since the bandwidth of these receivers is typically large. The distortion models can be derived by applying the full distortion model in (1), however, it will be too complex for implementation if not possible. In practice, fortunately, it is enough to consider up to the third-order distortions and the RF nonlinear model since the higher order-components are too small and can be omitted [15]. The output LNA then can be simplified as (3).

$$y_{RF}(t) = a_1 x_{RF}(t) + a_2 x_{RF}^2(t) + a_3 x_{RF}^3(t) \qquad (3)$$

The second-order component in (3) can be expressed as (4)

$$x_{RF}^2(t) = 2A^2(t) + x^2(t)e^{j2\omega_c t} + [x^*(t)]^2 e^{-j2\omega_c t} \qquad (4)$$

where $2x(t)x^*(t) = 2A^2(t)$ is the component around the baseband.

In (4), the distorted components appear at 0 and $\pm 2\omega_c$, but none appears at ω_c. This guarantees that the generated distortion does not affect itself and the adjacent but it does affect channels around $2\omega_c$.

The third component in (3) in turn can be represented as

$$a_3 x_{RF}^3(t) = a_3\{x^3(t)e^{j3\omega_c t} + [x^*(t)]^3 \cdot e^{-j3\omega_c t} + 3A^2(t) \cdot x(t)e^{j\omega_c t} + 3A^2(t)x^*(t)e^{-j\omega_c t}\} \quad (5)$$

As can be seen from (5), the distortion frequencies around ω_c generated by component $3A^2(t)x(t)e^{j\omega_c t}$ affects itself and the adjacent channels while the component $x^3(t)e^{j3\omega_c t}$ affects channels around $3\omega_c$.

As illustrated in Fig. 3, when the input signal has two frequencies components (f_1, f_2), the output signal will have two harmonic groups: $n \times f_1$, $m \times f_2$, and intermodulation $n \times f_1 \pm m \times f_2$. The distortion happens as soon as those components appear near the received signal frequency. For example, components $(2f_1 - f_2)$ and $(2f_2 - f_1)$ could distort f_1 and f_2. The other harmonics and inter-modulation, on the other hand, could distort other high-frequency signals.

2.2. Experimental Measurement of LNA nonlinear Distortion and Characteristics

To verify the derived models in the previous Section, we have conducted measurements on a commercial LNA from Minicircuits [16]. This LNA is suitable for wideband receivers, which is characterized by a low noise figure and an adequate gain factor. It also experiences very little variation within the receiver's frequency range. Indeed, from the provided experimental results in the datasheet, the amplification coefficient ZFL-500LN+ varies less than 0.7dB with the frequency range from DC to 500MHz [16]. We further measured with input signals at frequencies 50 MHz, 150 MHz, and 450 MHz. The results show that the characteristics including the linear amplification, the 2nd-order, and 3rd-order nonlinearity at all 3 frequencies are almost the same (Fig. 4) across the frequencies. This result indicates the working frequency mostly does not affect the LNA parameters and model.

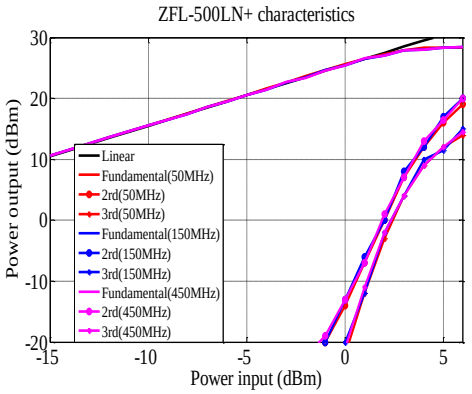

Fig. 4. ZFL-500LN+ parameters with different input frequency (50MHz, 150MHz, and 450MHz)

For the multichannel test case, we generated two channels of QPSK signals at frequencies of 5.3 Mhz and 5.8 Mhz using E8267D [17] and fed into the LNA inputs. The spectrum at the LNA output is shown in Fig. 5. From the figure, it is clear that the LNA nonlinear distortion affects the receiver channels at the signal frequency and frequencies of their harmonic and intermodulation. Specifically, with that QPSK inputs, multiple undesired frequency components appear at frequencies around 5.5 Mhz and also at 11 MHz and at 16.5 MHz. These measurement results are well-matched with the LNA distortion models in (4) and (5).

The experimental measurements are then fitted with the polynomial in (3) to extract the ZFL-500LN coefficients (i.e., a_i {i=1,2,3}). We adopted those realistic parameters set for our further simulation in this work.

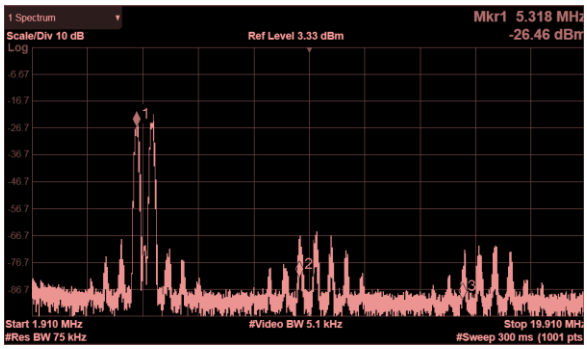

Fig. 5. ZFL-500LN+ RF output signal spectrum with 2 QPSK channels

3. LNA Distortion Compensation in Multichannel DRFs Using Reference Receiver

3.1. Structure of DRFs With Reference Receiver

As presented in Section II, due to LNA nonlinearity, the distortion components created by high input power channels will distort the signal themselves and other channels. This can lead to inaccurate reception of the low power channels. Therefore, it is required to have a compensation circuit that can effectively detect/estimate the unwanted distortion and remove them from the received signal.

The structure of the proposed receiver comprises the main receiver and a reference receiver, as depicted in Fig. 6 and Fig. 8. The former has the structure of a typical DRF with an LNA to ensure efficient sensitivity. Hence, the signal before ADC is already distorted by the LNA nonlinearity. In contrast, the signal in the reference receiver is considered linear due to the absence of the LNA. The received signals from the main receiver are then linearized by the distortions compensation circuits before passing to the demodulator. The LMS algorithm [18] is used to construct the adaptive distortion removal model. The linear reference signal will be used for calculating the nonlinear coefficients and then reproducing the harmonics and intermodulation components. During the distortion removal processing, the interested signal is recovered by either subtracting (ADS) or inverting (ADI) those distortion components. The main difference between the two methods is that the reproduced coefficients of LMS in ADS reflect the LNA characteristic, while those coefficients in ADI represent the inverse of LNA characteristics. In this work, the effect of quantization noise on the compensation process is also evaluated. Besides, the variable stepsize LMS for both methods is also considered for enhancing the compensation results. These processes are detailed in the following.

3.2. Adaptive Distortion Subtraction Technique

Fig. 6. and Fig. 7 depict the distortion cancellation scheme using the adaptive subtraction method ADS. With this scheme, the signal from the main receiver y_{RF} is the reference for the LMS algorithm. As the process converges, the coefficients $\widehat{w}_i$ of the LMS will be asymptotic to the distortion coefficients of the LNA. Assume that the signal received from the antenna after going through LNA, the ADC is (6)

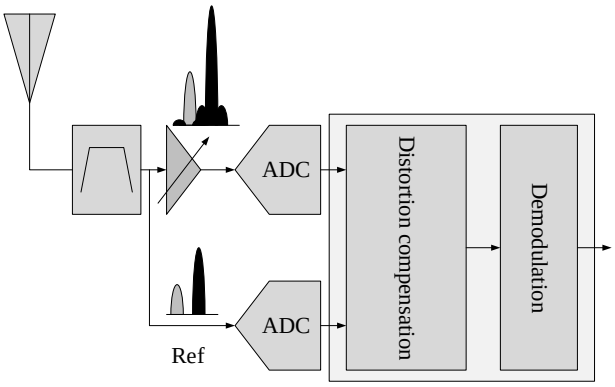

Fig. 6. Structure of the DRF with using reference receiver and distortion compensation circuit.

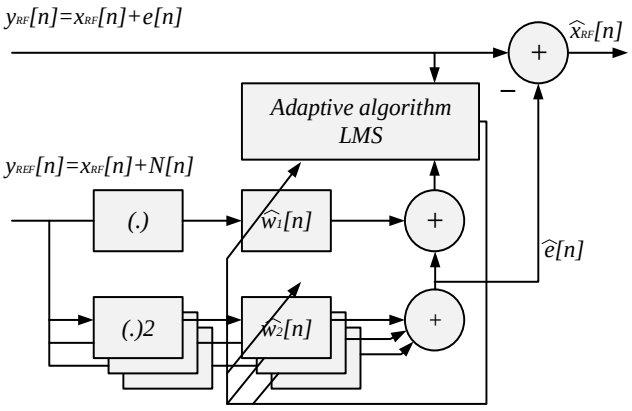

Fig. 7. Adaptive Distortion Subtraction Scheme in DRF

$$y_{RF}[n] = \sum_{i=1}^{k} w_i \cdot f_i(x_{RF}[n]) = a_1 x_{RF}[n] + e[n] \quad (6)$$

where $a_0$is the gain coefficient of LNA and n is the sampling sequence index, $f_1(x[n]) = a_1 x_{RF}[n]$ is the linear component (received signal), $f_{\mathrm{i}}(x[n]) = w_i x_{RF}^{\mathrm{i}}[n], i = 2,3 \ldots$ are the distortion components, $w_i[n]$ is the *i*-order coefficient.

Accordingly, the total distortion components in (6) is

$$e[n] = \sum_{i=2}^{k} w_i f_i(x_{RF}[n]) \quad (7)$$

From the linear reference channel, the reproduced distortion $\hat{e}[n]$ is expressed as

$$\hat{e}[n] = \sum_{i=2}^{k} \widehat{w}_i f_i(x_{RF}[n] + N[n]) \quad (8)$$

where $N[n]$ is the quantization noise of ADC, which can be assumed to be very small compared to the received signal ($rms(N^2) \ll rms(x_{RF}^2)$. The distortion canceling circuit (Fig. 7) subtracts the distorted RF signal from the reproduced distortion components recovered from the linear channel

$$\begin{aligned} \hat{x}_{RF}[n] &= a_1 x_{RF}[n] + e[n] - \hat{e}[n] \\ &= a_1 x_{RF}[n] + \sum_{i=2}^{k} w_i f_i(x_{RF}[n]) \\ &\quad - \sum_{i=2}^{k} \widehat{w}_i f_i(x_{RF}[n] + N[n]) \end{aligned} \quad (9)$$

From (9) it can be seen that the signal after the distortion compensation circuit, $\hat{x}[n]$, is approaching x[n] as long as high-order coefficients $\widehat{w}_2[n]$, $\widehat{w}_3[n]$, ... $\widehat{w}_{\mathrm{k}}[n]$ in (8) are getting close to $w_2[n]$, $w_3[n]$, ... $w_{\mathrm{k}}[n]$ in (7). This assymtotically process is achieve by adopting LMS algorithm, where the nonlinear coefficients are gradually adjusted as

$$\widehat{w}_i[n] = \widehat{w}_i[n-1] + \mu_i f_i(x[n]) \hat{\varepsilon}[n], \quad i = 1,2 \ldots k \quad (10)$$

where $\hat{\varepsilon}[n]$ and $\mu_i \{i = 1 - \mathrm{k}\}$ are LMS step sizes. $\hat{\varepsilon}$ is the estimated error and is expressed as:

$$\hat{\varepsilon}[n] = y_{RF}[n] - \sum_{i=1}^{k} \widehat{w}_i f_i(x_{RF}[n]).$$

Considering that, $f_{\mathrm{i}}(x[n]) = a_i x_{RF}^{\mathrm{i}}[n]$, are small enough to ignore with *i* > *3*, then the nonlinear coefficients at the convergence state is described as

$$\begin{aligned} w_1[n] &\to a_1 - 2a_2 N[n] \\ w_2[n] &\to a_2 \\ w_3[n] &\to a_3 \end{aligned} \quad (11)$$

The RF signal after the compensation process:

$$\begin{aligned} \hat{x}_{RF}[n] \approx a_1 x_{rf}[n] - (2a_2 x_{rf}[n] \\ + 3a_3 x_{rf}^2[n]) N[n] \end{aligned} \quad (12)$$

Equation (12) shows that the accuracy of the output signal $\hat{x}_{RF}[n]$ depends on the quantization noise N[n] of the ADC. From the equation, the quantization level directly defines the background noise (i.e., the scalar component) in the model.

3.3. Adaptive Distortion Inversion Technique

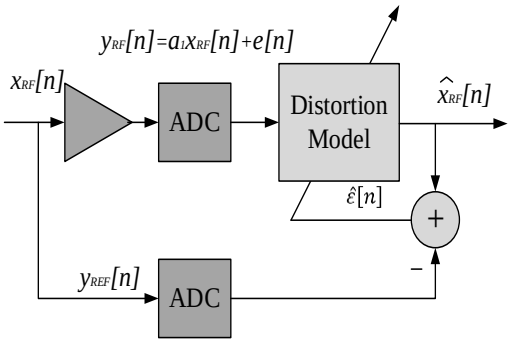

Fig. 8. Adaptive distortion inversion technique in DRF receiver.

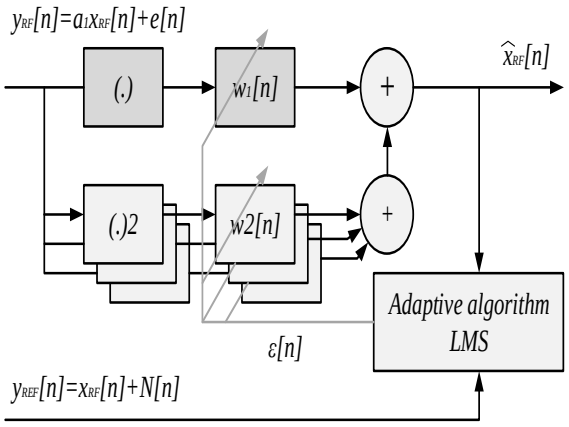

Fig. 9. Compensation circuit using an adaptive distortion inversion (ADI) algorithm.

Another method to extract the useful signal from its distortions is to invert all distortion components ADI [14]. The structure and detailed circuit of the compensation circuit using this technique are presented in Fig. 8, 9, respectively. In contrast to ADS, the signal from the main receiver $y_{RF}[n]$ is fed directly to the nonlinear compensation circuit while the reference signal $y_{REF}(n)$ is passed to the LMS circuit to adjust the compensation coefficients. With this scheme, the linear signal $y_{REF}(n)$ from the second branch will be the reference signal of the LMS, and the coefficients $\widehat{w_i}$ of LMS after converging will be the inverse of the LNA coefficients.

Let's denote $g_i(x[n])$ is the *i*-th order of the main receiver input $y_{RF}[n]$, thus

$$g_i(y_{RF}[n]) = y_{RF}^i[n], \text{ i = 1,2,…k} \quad (13)$$

The output of the compensation circuit expressed as (14)

$$\hat{x}_{RF}[n] = \sum_{i=1}^{k} (\widehat{w}_i) g_i(y_{RF}[n]) \quad (14)$$

This output is fed back to the LMS block, where it is subtracted from the reference input $y_{REF}(n)$ for calculating the model error

$$\begin{aligned} \hat{\varepsilon}[n] &= y_{REF}(n) - \sum_{i=1}^{k} \widehat{w}_i g_i(y_{RF}[n]) \\ &= x_{RF}[n] + N[n] - \sum_{i=1}^{k} \widehat{w}_i g_i(y_{RF}[n]) \end{aligned} \quad (15)$$

Based on the value square error $\hat{\varepsilon}[n]^2$ in (15), the LMS circuit dynamically adjusts the nonlinear coefficient $\widehat{w}_i[n]$ of the compensation circuits:

$$\widehat{w}_i[n] = \widehat{w}_i[n-1] + \mu_i f_i(y_{RF}[n]) \hat{\varepsilon}[n] \quad (16)$$

This process would continue until all components are converged to a fixed value, at that time the square error reaches the minimum. After the LMS converged, the generated output $\hat{x}_{RF}[n]$ would eventually approach the linear reference input $y_{REF}(n)$. In other words, the transfer function of the compensation circuit is the inverse of the LNA's transfer function. This helps to compensate for all non-linear components caused by LNA while keeping the signal level adequate for further processing at the digital domain.

Taking the same assumption, high order distortion with i > 3 can be ignored, from (15) the coefficients of the nonlinear model when convergence are shown in (17)

$$\begin{aligned} w_1[n] &\to {}^1/_{a_1} \\ w_2[n] &\to -\frac{a_2}{a_1} \\ w_3[n] &\to \frac{-a_1 a_3 + 2a_2^2}{a_1^3} \end{aligned} \quad (17)$$

The RF signal after the inverse process:

$$\hat{x}_{RF}[n] \approx x_{rf}[n] \quad (18)$$

Equation (18) shows that the signal $\hat{x}_{RF}[n]$ after correction has no explicit scalar noise component depending on the ADC quantization noise N[n]. However, the quantization noise in (16) could implicitly affect the precision of estimated nonlinear coefficients.

3.4. Variable stepsize LMS

Apart from the ability to accurately recover the received weak signal from the noise, the convergence speed of ADI and ADS is another important performance metric. As in some prior work [12-14], there is an inevitable trade-off between model accuracy and convergence time. The latter essentially depends on the step-size μ of the LMS algorithm.

To improve the convergence speed and the efficiency of the LMS algorithm, in this Section we propose to use a more flexible LMS with the stepsizes for each loop that can be and adjusted (herein referred to as VLMS). Principally, the step size is recalculated based on the current LMS model error. When the error is large (e.g., at the very beginning), fast adaption with larger step-size is required to accelerate the convergence. Once the model is close to convergence, i.e., the error is small, a slow adaption is needed to ensure a high level of accuracy. The adjustment step of LMS is gradually reduced according to the model error during the adaptive process.

The VLMS can be practically implemented as described in the following. The values of the step-size μ for LMS is updated as

$$\mu[n+1] = \mu_{min} + \frac{\mu_{max}}{\hat{\varepsilon}_{max}} \hat{\varepsilon}[n] \qquad (19)$$

where μ_{max} is the largest μ value that LMS, that is empirically set from the beginning, and $\hat{\varepsilon}_{max}$ is the initial difference of the reference signal and the distortion correction, which normally is the highest value at the first iteration.

The VLMS algorithm starts with large initial step size, relevant to the large error. Then during the convergence process, the stepsizes μ[i] will gradually decrease and stabilize. The step size models for VLMS coefficients are different between ADS and ADI, due to the differences in the error ranges.

4. Evaluation of The Distortion Compensation Schemes On Multichannel DRF receiver

To evaluate the distortion reduction effect of the schemes described in the previous Sections (i.e. ADS and ADI), we implemented the DRF model operating at the band UHF [19, 20]. The major performance metrics, including the convergence time of LMS and VLMS, ACRP and BERs have been tested. A pair of the same high-speed ADCs are used for directly digitalizing the RF signal for the main and reference channels.

In the simulation, four QPSK channels with a data rate for each channel of 4 Mbps are implemented. The parameters of the channels are given as in Table 1. Three channels causing distortion are channels with the carrier frequency $f_1 = 225\,MHz$ (Ch1), $f_2 = 430\,MHz$ (Ch2) and $f_3 = 440$ MHz (Ch3). The small power channel is channel Ch4 with a carrier frequency of and $f_4 = 450$ MHz.

4.1. LMS Convergence Speed

The first analyzed metric is the convergence speed of the implemented LMS circuits. Fig. 10(a)–(b) plot the convergence process of the LMS coefficient $\widehat{w}_i[n]$ for both LMS and VLMS. For LMS the fixed stepsize u is selected to be 0.002, 0.01, 0.05. For VLMS variable step size is modeled separately for ADI and ADS schemes. As can be seen from the figures, with both ADS and ADI, the larger the step size, the faster the convergence time will be, but the accuracy will decrease.

Both compensation solutions converge achieve convergence after a sufficient number of samples, where ADI tends to converge faster than ADS (e.g., with the step size $\mu = 0.002$, ADI requires ~10^5 samples while ADS requires ~10^6 samples).

When 1 GHz sample clock frequency is used, the actual convergence time is just a few milliseconds and will not be an issue for low bit-rate channels. However, the convergence characteristic, in this case, is estimated under the stationary input power.

Table 1. Simulation setup for RF channels

Channel	Type	Symbol rate/Input power level	RF Carry Frequencies
Ch1	QPSK	4 Mbps/-25 dBm	$f_{RF1} = 225$ MHz
Ch2	QPSK	4 Mbps/-25 dBm	$f_{RF2} = 430$ MHz
Ch3	QPSK	4 Mbps/-25 dBm	$f_{RF3} = 440$ MHz
Ch4	QPSK	4 Mbps/[-74÷-58 dBm]	$f_{RF4} = 450$ MHz

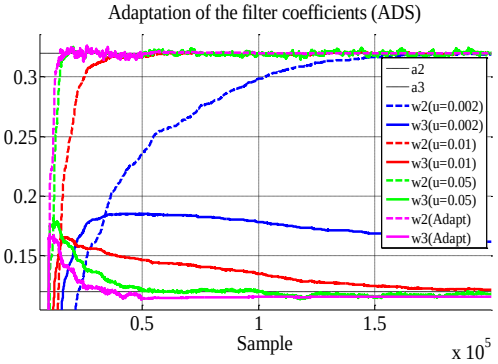

(a)

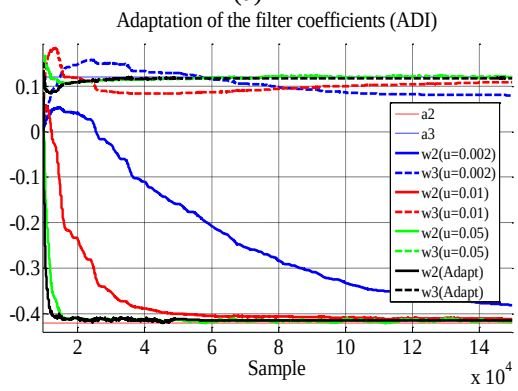

(b)

Fig. 10. The convergence of the nonlinear coefficients for (a) ADS and (b) ADI (a_i is the actual non linear parameters of the LNA and w_i $(i = 2, 3)$ is the LMS model parameters).

Under the dynamic input power (or SNR), the slow convergence speed could severely affect the performance of the adaptive circuit and the whole system. In such cases, the VLMS shows its advantages. Indeed, from the same figures, it is quite clear that VLMS exhibits much faster convergence speed. In this particular setup, VLMS in both ADI and ADS converge after 4.10^4 and 5.10^4 samples, i.e., about 10-100 times faster than the fixed step size LMS.

4.2. ACPR

Furthermore, the compensation effect is evaluated in the frequency domain. The spectra of the LNA output signal before and after the compensation are shown in Fig. 11.

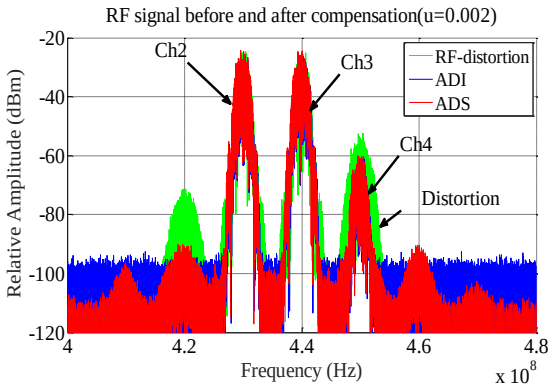

Fig. 11. Spectra of the RF signals without and with applying ADS or ADI compensation schemes at fixed LMS step size of 14 bit ADC.

With the carrier frequencies and channels' power selected in Table 1, Ch4 will be seriously affected by the distortion of the other three channels. From the spectra plot, Ch4 is distorted by the second harmonic generated by Ch1 (i.e., $f_{RF4} = 2f_{RF1}$) and the third-order intermodulation component generated by Ch2 and Ch3 (i.e., $f_{RF4} = 2f_{RF3} - f_{RF2}$).

Also from Fig. 11, the distortion is visibly mitigated by both ADS and ADI solutions. Regarding the background noise, ADS tends to have a higher noise floor than that of ADI,

which is consistent with the predictive models in (12) and (18). In contrast, ADI output naturally exhibits higher distortion levels than that of ADS. This may be intuitively explained by the fact that the ADS approximates the LNA model, which is a polynomial, by a polynomial while the ADI circuit reconstructs the polynomial form of the LNA inverse transfer function. The latter does not always guarantee a good level of accuracy compared to the former.

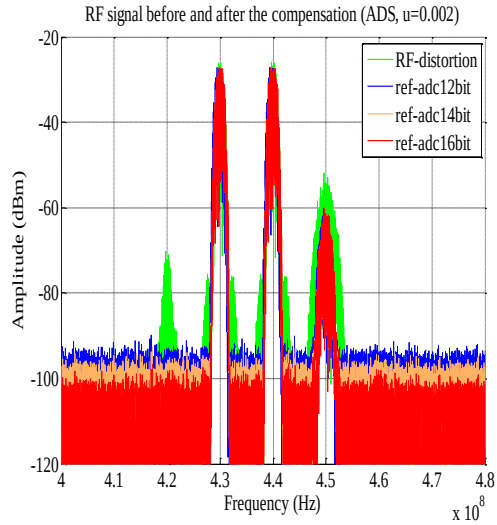

(a)

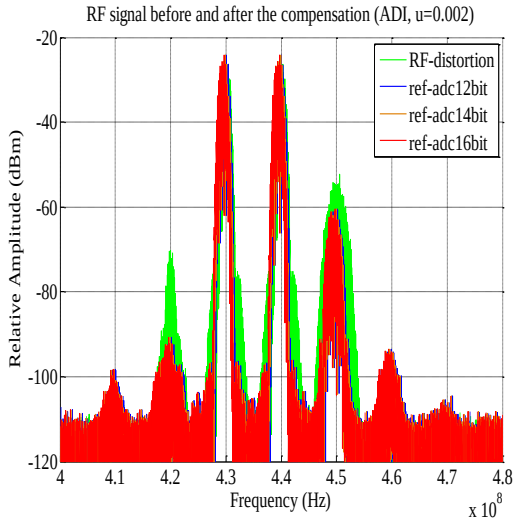

(b)

Fig. 12. Spectra of the RF signals with applying (a) ADS and (b) ADI

To quantify the compensation circuits and methods, we have measured the ACPR of the output signals and BER. The simulation has been conducted different quantization errors by using ADC with three levels of dynamic range, i.e., with 12 bit, 14 bit, and 16-bit ADCs. The results are evaluated for both ADI, ADS with both fixed and variable step sizes.

The ACPR index for Ch4 presented in Table 2 indicates that the ADS, in general, is slightly better than ADI regardless of the ADC dynamic range. It is also notable that ACRP of ADI does not improve with an increase in the ADC resolution while ACRP of ADS is getting better as soon as the quantization noise becomes smaller (Fig. 12)

Table 2. ACPR at the output of the compensation circuit of channel ch4

ADC resolution	12 bit	14 bit	16 bit
ACPR_ADS	-35 dBc	-37 dBc	-40 dBc
ACPR_ADI	-33 dBc	-33dBc	-33 dBc

Spectra in Fig. 12(a)–(b) support the above observation and show a clear difference between ADI and ADS. Indeed, the noise floor of the ADS is inversely proportional to the ADC resolution while that of ADI not only is lower but weakly dependent on the ADC resolution. After the compensation process, Ch4 distortion components in ADI are larger than those of ADS, this confirms the fact that ADS is more accurate than ADI as discussed earlier.

4.3. BER

Finally, the most important performance parameter, BER, is considered. The BER measurements have been conducted under the dynamic condition of the input power of channel Ch4, which varies in the range [-74 dBm to -58 dBm]. The input powers of the three other channels are chosen to be constant and equal -25 dBm, i.e., much larger than Ch4, therefore, the total input power is considered unchanged, so is the nonlinear characteristic of

LNA. BERs calculated for the receiver with and without the compensation circuit for 65 million of QPSK samples, with LMS and VLMS are plotted in Fig. 13. From the figure, it is notable that all compensation approaches significantly improve the BER as compared to the non-compensated receiver. Indeed, the BER of the Ch4 without the compensation is above 0.4, which is extremely high, i.e., cannot even meet the minimum requirement for any communication system. By applying either ADS or ADI compensation circuits, the BER of Ch4 has been improved by 2-3 orders of magnitude. We also observed from Fig. 13 that the ADS slightly outperforms ADI. Thus, it can be concluded that the performance of the DRF mainly depended on the accuracy of the adaptive compensation. In this case, ADS has better accuracy and results in lower BER while higher quantization noise in ADS does not degrade much of its BER performance.

Besides, when comparing LMS and VLMS, from Fig. 13, VLMS in both ADI and ADS enhances the performance of the compensation schemes compared to the fixed LMS. As we have discussed earlier, the fast convergence eventually helps to reduce the bit errors. Also from the BER plot, the impact of VLMS using ADS is quite clear for the entire considered power range, while the effect of VLMS on ADI is not clear as the improvement is only noticeable in the high input power range.

Finally, we evaluate BER under the dynamic input power, the same simulation setup was adopted with longer running time. Specifically, during the evaluation, the power of Ch1, 2, 3 were changed from $-25\,dBm$ for the first 185 million samples, then they are increased to $-21\,dBm$ for the next 130 million samples. Accordingly, the working point of LNA is dynamically changed and the signal-to-noise for Ch4 is also changed. In both ADS and ADI cases, VLMS works more effectively than normal LMS. In detail, VLMS has improved BER from $5.0\text{x}10^{-3}$ to $3.9\text{x}10^{-3}$ for ADS and from $6.7\text{x}10^{-2}$ to $5.2\text{x}10^{-2}$ for ADI.

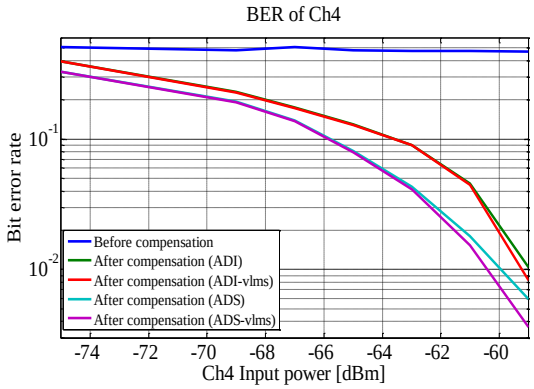

Fig. 13. BER calculated for channel Ch4 with ADS and ADI schemes with stationary input power.

5. Conclusions

In this paper, we analyzed in detail two solutions of LNA linearization in the DRF receiver. The processes are implemented at the RF domain by inverting and subtracting distortion information, calculated by using a linear reference receiver. The influence of the quantization noise of the linear reference receiver channel is included for evaluation. Distortion processing time is improved compared to the previous solutions.

Simulations are performed with 4 QPSK channels and all 3 high energy channels generate nonlinear distortions that affect the small energy channel Ch4. In this extreme case, the BER of channel Ch4 still improves by 2-3 orders. With the use of VLMS, the convergence time of the processing algorithm does not exceed 2.10^4 samples, which is hundreds of times faster than the conventional approach. The effect of the quantization noise of the reference ADC is more evident on ADS than ADI. When changing the 12 bits reference channel ADC to 16 bits, the ACPR of ADS is improved by 5 dB but the ADI hardly changes. All simulation results with selected parameters show that the ADS solution is better than ADI when regarding the quantization noise.

Acknowledgement

This research is funded by the Vietnam National Scientific Research under grant Project number ĐTĐLCN.33/17.

References

[1] O. Jamin, Broadband Direct RF Digitization Receivers, Analog Circuits and Signal Processing, Springer International Publishing Switzerland 121 (2014) 39-97. https://doi.org/10.1007/978-3-319-01150-9-2.

[2] L. Anttila, M. Valkama, M. Renfors, "Circularity-based I/Q imbalance compensation in wideband direct-conversion receivers", IEEE Trans, Veh, Technol. 57(4) (2008) 2099-2113.

[3] Software Defined Radio, Spectrum Analyzer and Panoramic Adapter/ Available: http://www.rfspace.com/RFSPACE/SDR-IQ.html/, 2019 (accessed 20 May 2019).

[4] Perseus SDR - Software Defined 10 kHz - 30 MHz Receiver. Available: http://microtelecom.it/perseus/, 2019 (accessed 20 May 2019).

[5] Jaakko Marttila, Markus Allénand Marko Kosunen, "Reference Receiver Enhanced Digital Linearization of Wideband Direct-Conversion Receivers" IEEE Transactions On Microwave Theory And Techniques 65(2) (2017) 607-620.

[6] R. Vansebrouck, O. Jamin, P. Desgreys, V.-T. Nguyen, "Digital distortion compensation for wideband direct digitization RF receiver", in Proc. IEEE 13th Int, New Circuits Syst, Conf, (NEWCAS), Jun, 2015, pp. 1-4.

[7] Raphaël Vansebrouck, Chadi Jabbour, Olivier Jamin, and Patricia Desgreys, "Fully-Digital Blind Compensation of Non-Linear Distortions in Wideband Receivers" IEEE Transactions OnCircuits And Systems-I: Regular Papers 64(8) (2017) 2112-2123.

[8] M. Grimm, M. Allen, J. Marttila, M. Valkama, R. Thoma, "Joint mitigation of nonlinear rf and baseband distortions in wideband direct-conversion receivers", Microwave Theory and Techniques, IEEE Transactions on 62(1) (2014) 166-182.

[9] A.A. Abidi, "Direct-conversion radio transceivers for digital communications", IEEE J. Solid-State Circuits. 30(12) (1995) 1399-1410.

[10] O. Jamin, V. Rambeau, F. Goussin, G. Lebailly, "An rf frontend for multi-channel direct rf sampling cable receivers", ESSCIRC (ESSCIRC), Sept 2011, pp. 347-350.

[11] B. Razavi, "Design considerations for direct-conversion receivers", IEEE Trans. Circuits Syst. II, Analog Digit. Signal Process. 44(6) (1997) 428-435.

[12] V.N. Anh, L.H. Nam, T.T.H. Tham, T.Q. Kien, "Novel Distortion Compensation Scheme for Narrowband Multi-channel Direct RF Digitization Receiver", 2019 19th International Symposium on Communications and Information Technologies (ISCIT'19), Sep, 2019.

[13] V.N. Anh, T.T.H. Tham, T.Q. Kien, L.H. Nam, "LNA Nonlinear Distortion Impacts In Multichannel Direct RF Digitization Receivers And Linearization Techniques", Research in Intelligent and Computing in Engineering 2019, Aug, 2019.

[14] V.N. Anh, L.H. Nam, T.T.H. Tham, T.Q. Kien, H.V. Phuc, "Adaptive Distortion Inversion Technique for LNA's Nonlinearity Compensation in Direct RF Digitization Receivers", 2019 International Conference on Advanced Technologies for Communications (ATC), Oct 2019.

[15] Gharaibeh, M. Khaled, Nonlinear distortion in wireless systems: modeling and simulation with MATLAB, John Wiley & Sons Ltd, 2012.

[16] ZFL-500LN+ http://www.minicircuits.com

[17] Keysight, "E8267D PSG Vector Signal Generator, 100 kHz to 44 GHz" Available: https://www.keysight.com/en/pdx-x202238-pn-E8267D/psg-vector-signal-generator-100-khz-to-44-ghz?cc=VN&lc=eng/, 2020 (accessed 18 June 2020).

[18] S. Haykin, Adaptive Filter Theory, 4th ed. Upper Saddle River, NJ, USA: Prentice-Hall, 2002.

[19] Aselsan, "PRC V/UHF SDR Handheld Radios." Available: https://www.aselsan.com.tr/en/capabilities/military-communication-systems/vuhf-military-radios/prc-vuhf-sdr-handheld-radios, May 2020.

[20] Jean Walrand, Pravin Varaiya, "High-Performance Communication Networks" (Second Edition), 2000.